Jurnal Ilmu Fisika
Vol. 17, No. 2, September 2025, pp. 157–170
ISSN: 1979-4657 (Print); 2614-7386 (Online)
https://doi.org/ 10.25077/jif.17.2.157-170.2025

Structural Evolution and Ionic Conductivity of Al_2O_3-Doped LLZO via Single Heat Treatment

Endah Yuniarti[1], Slamet Priyono[1,2], Simon Sindhu Hendradjaja[1], Jan Setiawan[2], Kusdi Prijono[3], Brity Femlee Ringkuangan[1]

[1]Department of Aeronautical Engineering, Air Chief Marshal Suryadarma Aerospace University, Jalan Protokol Halim Perdana Kusuma Komplek Bandara Halim Perdana Kusuma, Jakarta 13610, Indonesia
[2] Research Center of Advanced Material, National Research and Innovation Agency (BRIN), PUSPIPTEK Serpong 15314, Tangerang - Banten, Indonesia
[3]Advanced Chemical and Advanced Physics Imaging Laboratory - Directorate of Laboratory Management, Research Facilities and Science and Technology, National Research and Innovation Agency (BRIN), PUSPIPTEK Serpong 15314, Tangerang - Banten, Indonesia

Article Info

Article History:

Received January 24, 2025
Revised May 10, 2025
Accepted May 11, 2025
Published online June 06, 2025

Keywords:

$Li_7La_3Zr_2O_{12}$
LLZO:Al
Single Heat Treatment
Solid Electrolyte
Ionic Conductivity

Corresponding Author:

Endah Yuniarti,
Email: eyuniarti@unsurya.ac.id

ABSTRACT

This study investigates the synthesis via solid state reaction and characterization of $Li_7La_3Zr_2O_{12}$ (LLZO) as a solid electrolyte doped with Al_2O_3 using a one-step heat treatment (sintering at 900°C for 4 hours). Samples were prepared with doping variations; pure LLZO (0Al-LLZO), 0.25Al-LLZO, and 0.5Al-LLZO, based on the formula $Li_{(7-x)}Al_xLa_3Zr_2O_{12}$ with x = 0, 0.25, and 0.5, and were mixed using ball milling for 4 hours at 25 Hz. XRD and Rietveld refinement confirmed the formation of a dominant tetragonal $Li_7La_3Zr_2O_{12}$ phase alongside minor secondary phases. Grain sizes ranged from 1.2 to 1.3 µm, and densification improved with increasing Al content. The 0.25Al-LLZO sample exhibited the highest ionic conductivity of 2.83×10^{-9} S/cm at room temperature, representing a 2.96-fold increase over undoped LLZO. These results indicate that Al doping significantly enhances structural stability and Li-ion transport in LLZO electrolytes processed at moderate temperatures.

1. INTRODUCTION

The development of solid-state electrolytes is critical to advancing lithium-ion battery technology, driven by the need for greater energy density, safety, and efficiency (Han et al., 2020; Lotsch & Maier, 2017; Woolley & Vargas-Barbosa, 2022; Zhao et al., 2019). Unlike liquid electrolytes, which pose risks of leakage and flammability, solid-state electrolytes offer enhanced thermal stability and enable higher energy densities (Han et al., 2020; Luo et al., 2024; Zhao et al., 2019). $Li_7La_3Zr_2O_{12}$ (LLZO) is a promising garnet-type solid-state electrolyte due to its high ionic conductivity, chemical stability, and compatibility with lithium metal anodes (Ihrig et al., 2021; Il'ina et al., 2019; Lan et al., 2020; Raju et al., 2021; Sharifi et al., 2023; Wang College Park MD (United States)] et al., 2020). However, achieving its optimal phase and structure to maximize conductivity demands careful control of the synthesis process.

At present, various methods have been employed to synthesize LLZO, including sol-gel, hydrothermal, and solid-state reaction (SSR) methods (Raju et al., 2021; Yoon et al., 2017). Although sol-gel and hydrothermal methods offer better control over particle size and homogeneity, the SSR method remains widely used due to its simplicity, cost-effectiveness, and scalability. SSR can produce high-purity, structurally stable LLZO with competitive ionic conductivity, and enables effective doping, such as with Al_2O_3, to enhance electrochemical performance.

In recent years, significant advancements have been made in the development of lithium solid-state electrolytes, particularly through doping strategies, innovative synthesis methods, and the optimization of processing conditions (Li et al., 2024; Machín et al., 2024; S. Wang et al., 2025). Among the various approaches, doping with different cations has been reported to stabilize the cubic phase of lithium lanthanum zirconate (LLZO) and enhance its ionic conductivity. It has been shown that adjusting the synthesis conditions, such as sintering temperature and lithium concentration, plays a crucial role in controlling the structural integrity and performance of LLZO-based electrolytes (Salimkhani et al., 2021; Xue et al., 2018). Several studies have also implemented multistage heat treatment cycles to enhance phase purity and conductivity, as seen in the works of (Neises et al., 2022; Tsai et al., 2019; Xue et al., 2018). However, these methods often require temperatures exceeding 1000°C or prolonged sintering times, which can lead to lithium loss due to volatilization, ultimately degrading the ionic conductivity and overall material performance. (Montoya et al., 2024) investigated the formation of the secondary phase $La_2Zr_2O_7$ (LZO) during the c-LLZO sintering process at 1000°C for 1 hour. $La_2Zr_2O_7$ (LZO), which belongs to the pyrochlore structure, is known to be an insulating material both electronically and ionically.

There is limited research on synthesizing LLZO solid electrolytes using a single heat treatment. For instance, a study by (Kiyek et al., 2024) successfully synthesized LLZO and fabricated composite cathodes in a single step using the tape casting process and (Rangasamy et al., 2012) synthesized LLZO with various Al concentrations using a single-stage heat treatment at 1000°C for 4 hours. Therefore, the use of a single heat treatment method not only streamlines the LLZO synthesis process but also produces a material with properties comparable to those achieved through multi-stage processes, making it a more efficient and practical approach to produce solid electrolytes in lithium batteries.

Hence, this paper aims to present a novel solid-state method for synthesizing LLZO using a single heat treatment at a lower sintering temperature. This approach is compared to conventional solid-state reaction methods that involve multi-step treatments, which are more time-consuming and costly. The primary motivation of this study is to explore the solid-state synthesis of Al-substituted LLZO to enhance its ionic conductivity and phase stability and minimize lithium volatilization. The LLZO powder, doped with Al_2O_3, was synthesized under carefully controlled conditions, where both lithium concentration and calcination temperature were optimized to obtain a high-purity, single-phase material. The powder was sintered at a single temperature of 900 °C for 4 hours, and its structural and morphological properties were characterized using X-ray diffraction (XRD) and scanning electron microscopy (SEM). The electrical conductivity was evaluated through impedance spectroscopy (EIS). The findings from this study suggest that a single heat treatment process can be an energy-efficient and effective method for fabricating LLZO electrolytes with excellent structural and electrochemical properties, paving the way for potential applications in energy storage devices.

2. METHOD

2.1 Materials and Instruments

In this research, the solid electrolyte $Li_7La_3Zr_2O_{12}$ (LLZO) was synthesized with three variations: pure-LLZO, 0.25Al-LLZO, and 0.5Al-LLZO. The chemical composition formula is $Li_{(7-x)}Al_xLa_3Zr_2O_{12}$ with $x = 0;\ 0.25; 0.5$. The amount of the materials calculated per 15 grams is shown in Table 1. After the stoichiometric ratio was weighed, they were mixed using the ball milling process for 4 hours at 25 Hz to homogenize and refine the powder particles. The resulting powder was then dried in an oven at 70°C for 24 hours to eliminate moisture.

Table 1 Stoichiometric composition of precursor powders used for the solid-state synthesis of pure and Al-doped LLZO samples (based on a 15 g batch).

No.	Sample	Chemical composition (15 g)	Li_2CO_3 (g)	La_2O_3 (g)	ZrO_2 (g)	Al_2O_3 (g)
1.	Pure-LLZO	$Li_7La_3Zr_2O_{12}$	4.62	8.72	4.40	-
2.	0.25Al-LLZO	$Li_{6.75}Al_{0.25}La_3Zr_2O_{12}$	4.42	8.67	4.37	0.22
3.	0.5Al-LLZO	$Li_{6.5}Al_{0.5}La_3Zr_2O_{12}$	4.23	8.62	4.35	0.44

The ball milling process was conducted at the Research Center of Advanced Materials, National Research and Innovation Agency (BRIN), using the Planetary Ball Mill (MTI Battery Corp) instrument. Thermogravimetric/Differential Thermal Analysis (TG/DTA) to determine the appropriate sintering temperature range. The TG/DTA test was conducted at the Nanoscience and Nanotechnology Research Center Laboratory, ITB, using the TG/DTA Hitachi STA7300 instrument. Sintering process with an MTI Furnace. X-ray Diffraction (XRD) was employed to analyze the crystal phases in all sintered samples, using Malvern PAN analytical instrument with a Cu-Kα radiation source ($\lambda = 1.5418$ Å) with Bragg angles (2θ) between 5° to 80° (scan rate 3°/min). Scanning Electron Microscopy (SEM) to evaluate their microstructure was conducted using the FE-SEM FEI INSPECT F50 and JEOL-JED 2300.

2.2 Method and Procedure

The precursor powders for LLZO solid-state synthesis were homogenized via mechanical mixing using a planetary ball mill for 4 hours at a speed of 25 Hz (Figure 1a). The materials were placed in a zirconia milling jar with a diameter of 9 cm and zirconia balls with a diameter of 1 cm as grinding media (Figure 1b). A ball-to-powder weight ratio of 1:5 was employed to ensure efficient mixing of the components. As the milling proceeds, the balls collide with the powder, leading to a reduction in particle size and an increase in homogeneity. Continuous mechanical forces cause the particles to break apart and reassemble, enhancing solid-state diffusion and reducing crystallite size. The constant rotation of the grinding vessel ensures thorough mixing of the precursors, resulting in a fine, homogeneously distributed powder (Ma et al., 2024; Parascos et al., 2022; Wood et al., 2020). The LLZO powder is stored in an oven at 70°C prior to undergoing thermal analyses, including TG/DTA, and characterization tests such as XRD, SEM, and EIS.

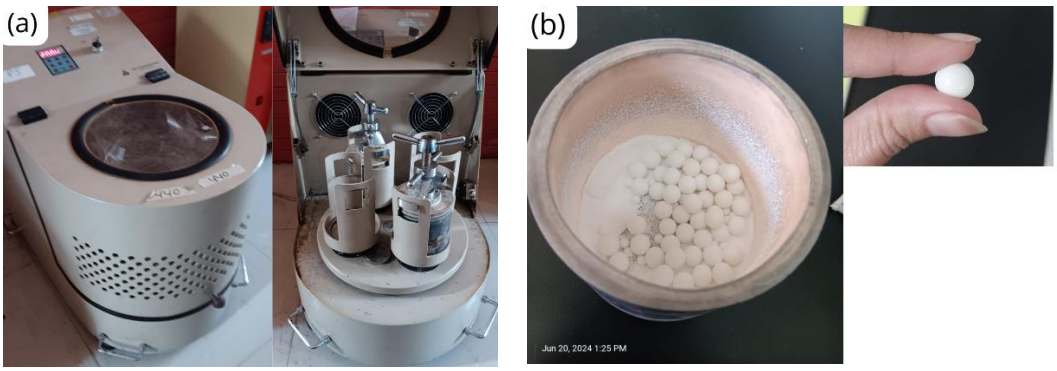

Figure 1 (a) Planetary ball mill equipment used for the homogenization of precursor powders in the solid-state synthesis of LLZO and the system consists of multiple rotating jars mounted on a central disk, (b) Zirconia milling jar and zirconia balls (diameter ~1 cm) used as the grinding media during the ball milling process.

The powder precursor produced was then analyzed using Thermogravimetric/Differential Thermal Analysis (TG/DTA) to determine the appropriate sintering temperature range. The TG/DTA test was conducted at the Nanoscience and Nanotechnology Research Center Laboratory, ITB, using the TG/DTA Hitachi STA7300 instrument. Prior to testing, the sample was heated in an oven at 70°C for 24 hours.

The LLZO powder doped with Al_2O_3 was sintered in an MTI furnace at 900°C for 4 hours, based on the DTA/TG analysis results. After the sintering process, the LLZO samples were characterized to evaluate their structural evolution, phase stability, and ionic conductivity. X-ray Diffraction (XRD)

was utilized to identify the crystal phases of the sintered samples, while Scanning Electron Microscopy (SEM) was employed to analyze grain morphology. Electrochemical Impedance Spectroscopy (EIS) was conducted to measure the ionic conductivity of the samples.

3. RESULTS AND DISCUSSION

3.1 Thermogravimetric/Differential Thermal Analysis (TG/DTA) Test

Based on Figure 2, the green DTA curve illustrates the changes in heat within the sample as the temperature rises. The exothermic and endothermic peaks are identified by variations in the shape of this curve. Endothermic peaks indicate heat absorption, typically associated with decomposition or phase transitions requiring energy. In Figure 2, the endothermic peak is observed in the region where the DTA curve shows a significant decline. Exothermic peaks represent energy release, often linked to crystallization or other exothermic chemical reactions, which are visible at the upward peaks of the DTA curve.

The blue TG curve reflects the reduction in sample mass as the temperature increases, which may indicate material decomposition or the evaporation of volatile substances. A sharp drop in the TG curve suggests a substantial weight loss at a specific temperature, indicating a chemical change in the LLZO material (Neises et al., 2022; Wu et al., 2023). The endothermic peak is seen in the low-to-mid temperature range of the DTA curve, potentially corresponding to the initial decomposition of organic compounds or a phase transition from LLZO to an intermediate phase. Meanwhile, the exothermic peak is represented by the upward peak in the DTA curve, signaling the formation of a stable LLZO crystal phase, accompanied by a flat TG curve in the high-temperature region (Montoya et al., 2024; Neises et al., 2022).

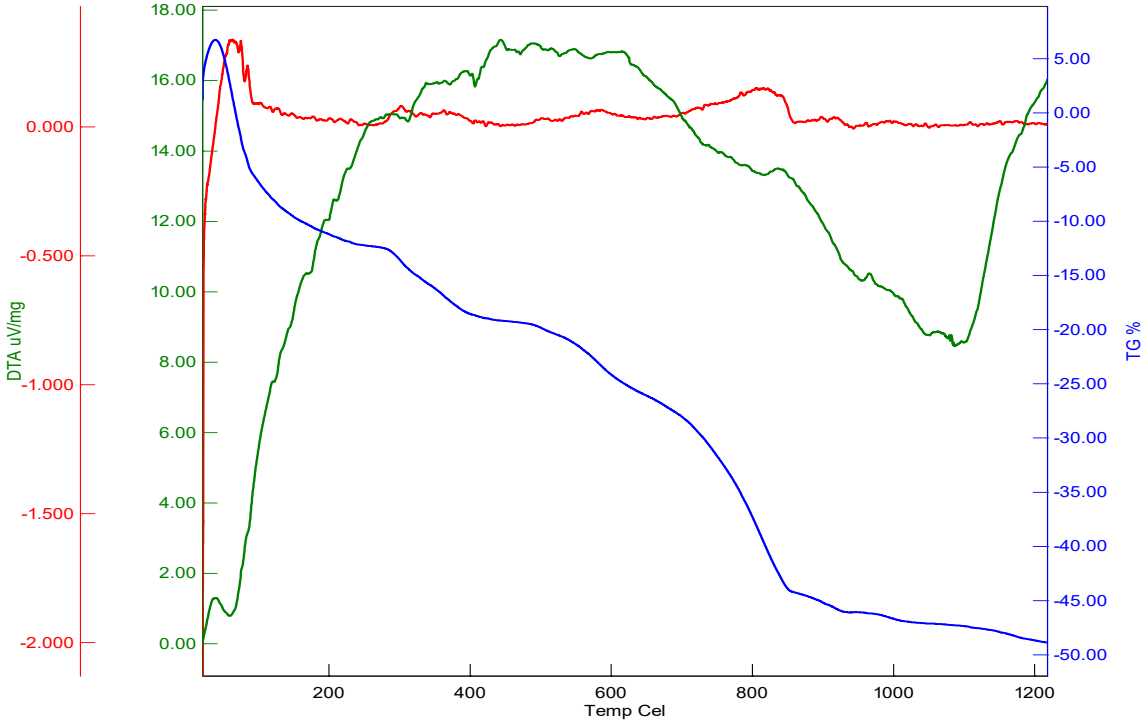

Figure 2 TG/DTA/DTG graph of the LLZO precursor sample with the blue curve represents the thermogravimetric (TG) profile, the green curve shows the differential thermal analysis (DTA), and the red curve corresponds to the differential thermogravimetric (DTG) data.

The mass of the powder precursor used for the TG/DTA test was 1.192 grams. The mass reduction observed in the TG curve, shown in Figure 2 and Table 2, occurred gradually across four temperature segments: 0°C–200°C, 200°C–600°C, 600°C–1000°C, and at temperatures above 1000°C,

where almost no further mass loss was detected. The stages of mass reduction in the TG curve are closely associated with the peaks observed in the DTA curve. To facilitate the identification of endothermic and exothermic peaks from the TG/DTA test results, the DTA curve was enlarged for each temperature range (0°C–200°C, 200°C–600°C, 600°C–1000°C, and >1000°C), as shown in Figure 3.

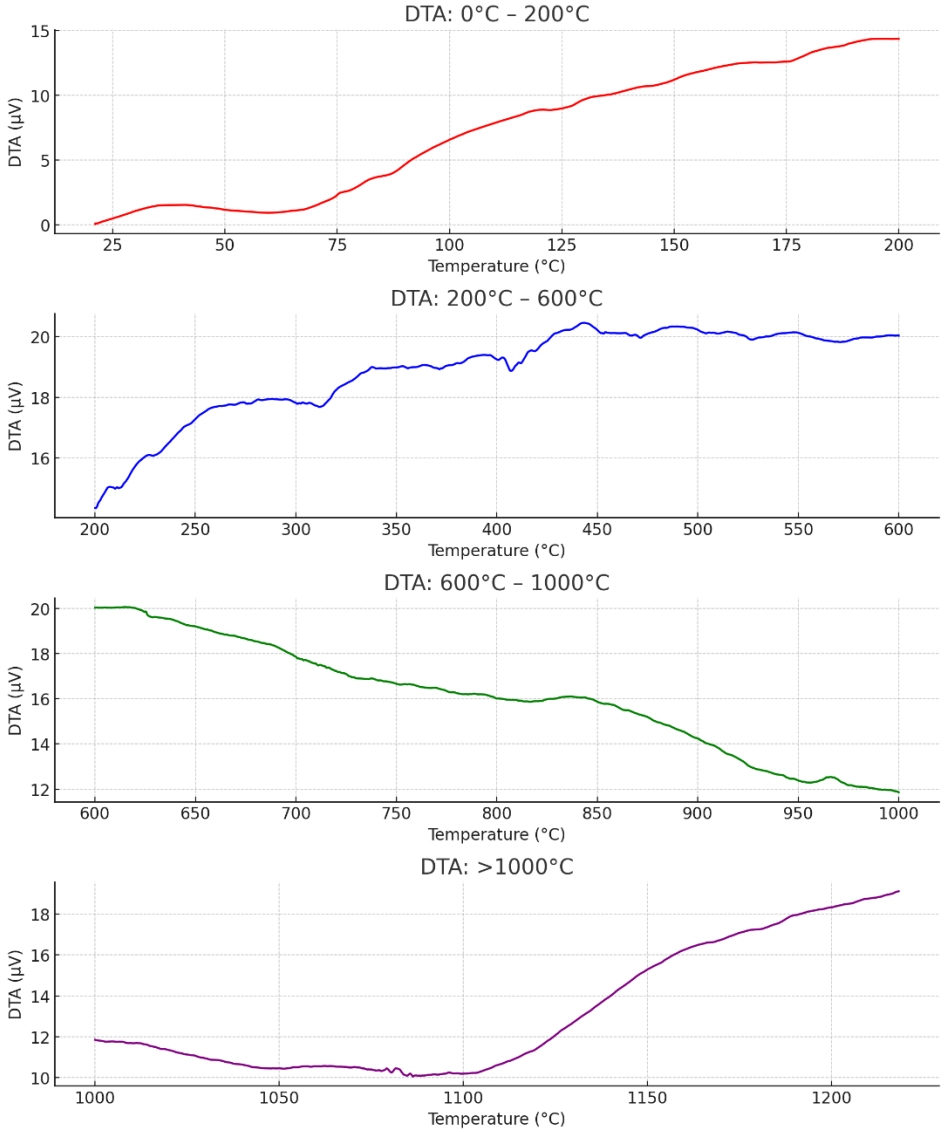

Figure 3 DTA curve in the temperature ranges 0°C – 200°C, 200°C – 600°C, 600°C – 1000°C, and >1000°C.

In the first temperature segment, ranging from 0°C to 200°C, a mass loss of 153.54 µg was observed, with an endothermic peak at 59.49°C. This endothermic peak indicates heat absorption, leading to an initial mass loss due to the evaporation of free water or solvents physically adsorbed on the particle surface. These volatile components, such as water or other molecules, are not chemically bonded to the LLZO precursor (Karuppiah et al., 2023; Parascos et al., 2022; Salimkhani et al., 2021). In the second temperature segment, from 200°C to 600°C, a mass loss of 154.46 µg occurred, and three endothermic peaks were observed at 210.29°C, 311.98°C, and 406.98°C. These peaks are associated with the decomposition of Li_2CO_3 (Lithium Carbonate) into lithium oxide and CO_2 gas, as reflected by the mass loss in the TG curve (Karuppiah et al., 2023; Parascos et al., 2022). In the third temperature segment, from 600°C to 1000°C, a larger mass loss of 268.32 µg was detected. The endothermic peak spans a broader temperature range, resulting in a less defined, sharper peak. However, a notable decrease is observed at 954.07°C, which is determined to be the endothermic peak. This stage is likely associated

with the further decomposition of more stable compounds, such as La_2O_3 (Lanthanum (III) Oxide) and ZrO_2 (Zirconium Dioxide), or the formation of a new LLZO phase. Typically, the material begins to form a more stable crystalline phase at higher temperatures. In this range, the graph shows an overall decrease, and an exothermic peak is observed, though it is not prominent (no sharp upward spike), at a temperature of 966.67°C. The presence of this exothermic peak suggests the formation of a new phase or the crystallization of LLZO. The formation of a new phase during the sintering process is generally exothermic, as the reorganization of the crystalline structure releases energy (Montoya et al., 2024; Parascos et al., 2022; Raju et al., 2021). Beyond 1000°C, there is minimal mass loss, only 26.27 µg, indicating that the solid-state reaction is likely complete, and the system has reached thermal stability. This suggests the LLZO phase is forming, or sintering is occurring, where particles fuse without further mass loss (Karuppiah et al., 2023; Parascos et al., 2022). In this temperature range, a noticeable increase in the graph is seen, corresponding to an exothermic peak between 1100°C and 1200°C, indicating significant heat release at these elevated temperatures (Wu et al., 2023).

Table 2 Summary of thermal events observed from the DTA/TG analysis of LLZO precursor powders, showing temperature ranges, peak types, corresponding mass loss, and associated processes during solid-state synthesis.

No.	Temperature Range	Type of Peak	Mass Loss (µg)	Assigned Process
1.	0°C–200°C	Endothermic peak at 59.49°C	153.54	Evaporation of free water or solvents physically adsorbed on the particle surface.
2.	200°C–600°C	Endothermic peaks at 210.29°C, 311.98°C, and 406.98°C	154.46	Decomposition of Li_2CO_3 (Lithium Carbonate) into lithium oxide and CO_2 gas.
3.	600°C–1000°C	Endothermic peak at 954.07°C	268.32	Decomposition of more stable compounds, such as La_2O_3 (Lanthanum (III) Oxide) and ZrO_2 (Zirconium Dioxide), the formation of a new LLZO phase.
4.	>1000°C	Exothermic peak between 1100°C and 1200°C	26.27	The solid-state reaction is considered complete, indicating the formation and crystallization of the LLZO phase.

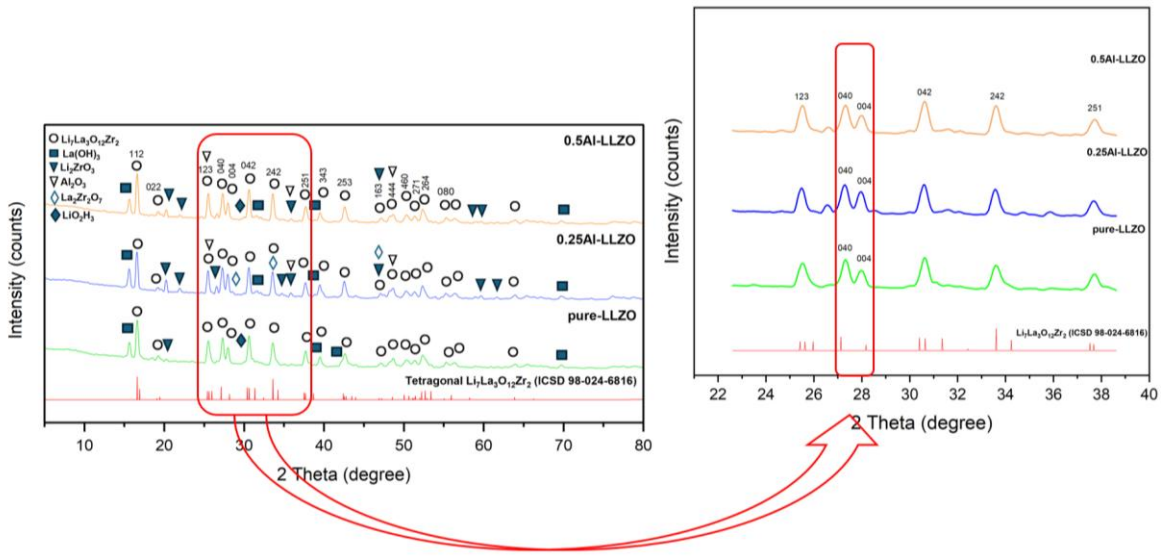

Figure 4 XRD patterns of pure LLZO, 0.25Al-LLZO, and 0.5Al-LLZO samples synthesized via solid-state reaction, compared with standard patterns of tetragonal $Li_7La_3Zr_2O_{12}$ (ICSD 98-024-6816). The magnified region (right) between 2θ = 22° and 40° highlights key diffraction peaks for phase identification, particularly the splitting of peaks at 2θ = 27.6° indicative of the tetragonal LLZO structure.

3.2 Crystallographic Analysis of LLZO:Al Solid Electrolyte Material using X-Ray Diffraction (XRD)

The X-Ray Diffraction (XRD) analysis was performed on LLZO:Al samples sintered at 900°C for 4 hours. The phases identified from the XRD test results are shown in Figure 4. For all variations of LLZO:Al samples (pure-LLZO, 0.25Al-LLZO, and 0.5Al-LLZO), the following phases were identified: $La_3Li_7Zr_2O_{12}$, $La(OH)_3$, Li_2ZrO_3, Al_2O_3, La_2ZrO_7, and LiO_2H_3. The diffraction pattern analysis was referenced to the Inorganic Crystal Structure Database (ICSD) with the following entries: $La_3Li_7Zr_2O_{12}$ phase (ICSD 98-024-6816), $La(OH)_3$ phase (ICSD 98-024-5670), Li_2ZrO_3 phase (ICSD 98-003-1941), Al_2O_3 phase (ICSD 98-060-8996), $La_2Zr_2O_7$ phase (ICSD 98-018-4090), and LiO_2H_3 phase (ICSD 98-003-5156).

The $La_3Li_7Zr_2O_{12}$ phase formed exhibits a tetragonal crystal structure. The presence of the tetragonal phase is indicated by the appearance of peak doublets, most notably around $2\theta = 27.6°$, as highlighted in Figure 4. This characteristic splitting is clearly observed in all three samples. For the pure-LLZO sample, the lattice parameters are $a = b = 13.06637$ Å and $c = 13.02689$ Å; for the 0.25Al-LLZO sample, the lattice parameters are $a = b = 13.09954$ Å and $c = 13.02492$ Å; and for the 0.5Al-LLZO sample, the lattice parameters are $a = b = 13.0814$ Å and $c = 13.00351$ Å. The $La(OH)_3$ phase formed exhibits a hexagonal crystal structure. For the pure-LLZO sample, the lattice parameters are $a = b = 6.528403$ Å and $c = 3.855959$ Å; for the 0.25Al-LLZO sample, the lattice parameters are $a = b = 6.55629$ Å and $c = 3.873637$ Å; and for the 0.5Al-LLZO sample, the lattice parameters are $a = b = 6.527525$ Å and $c = 3.85376$ Å. The Li_2ZrO_3 phase formed exhibits a monoclinic crystal structure. For the pure-LLZO sample, the lattice parameters are $a = 5.437387$ Å, $b = 9.020887$ Å, and $c = 5.429317$ Å; for the 0.25Al-LLZO sample, the lattice parameters are $a = 5.431582$ Å, $b = 9.026302$ Å, and $c = 5.426698$ Å; and for the 0.5Al-LLZO sample, the lattice parameters are $a = 5.432705$ Å, $b = 9.017407$ Å, and $c = 5.419316$ Å. The Al_2O_3 phase formed exhibits a hexagonal crystal structure. For the 0.25Al-LLZO sample, the lattice parameters are $a = b = 4.979389$ Å and $c = 12.701924$ Å, while for the 0.5Al-LLZO sample, the lattice parameters are $a = b = 4.820808$ Å and $c = 13.197142$ Å. The $La_2Zr_2O_7$ phase formed exhibits a cubic crystal structure, and this phase is only observed in the 0.25Al-LLZO sample, with lattice parameters $a = b = c = 10.742101$ Å. The LiO_2H_3 phase formed exhibits a monoclinic crystal structure. For the pure-LLZO sample, the lattice parameters are $a = 7.389879$ Å, $b = 8.309691$ Å, and $c = 3.191586$ Å; and for the 0.5Al-LLZO sample, the lattice parameters are $a = 7.421423$ Å, $b = 8.291054$ Å, and $c = 3.191913$ Å.

The refined lattice parameters can be used to calculate the theoretical density ρ_{theo} of the investigated material using the following formula:

$$\rho = \frac{ZM}{N_A abc} = \frac{ZM}{N_A a^2 c} \quad (1)$$

with Z being the number of formula units in the unit cell, M the molar mass, N_A the Avogadro constant ($6.022 \times 10^{23}\ mol^{-1}$), and a, b, c the lattice constant (tetragonal crystal structure have lattice parameters are $a = b$). The respective parameters for LLZO:Al is shown in Table 3.

Table 3 Parameters for LLZO: Al calculates the theoretical density ρ_{theo} with the lattice constant derived from XRD measurements, M the molar mass calculated from the molecular formula, Z the number of formula units in the unit cell

No.	Materials	Pure-LLZO	0.25Al-LLZO	0.5Al-LLZO
1.	$a = b$ (Å)	13.06637	13.099536	13.0814
2.	c (Å)	13.02689	13.024921	13.003505
3.	$M\ (g/mol)$	839.75	844.77	849.77
4.	Z	8	8	8
5.	$\rho\ (g/cm^3)$	5.02	5.02	5.07

The stability of the cubic phase of $Li_7La_3Zr_2O_{12}$ (LLZO) is highly dependent on lithium stoichiometry. During high-temperature processing, the high volatility of lithium presents a major challenge, especially at temperatures exceeding 1000°C, leading to lithium loss and disrupting the desired cubic phase stability (Heywood et al., 2022; 2023). Lithium evaporation at high temperatures contributes to the formation of secondary phases such as $La_2Zr_2O_7$ (LZO), which is both electronically and ionically insulating, thereby reducing the overall ionic conductivity of LLZO(Montoya et al., 2024). Moreover, LLZO is unstable in air, where Li^+/H^+ exchange reactions can lead to the formation of a hydrophobic surface layer composed of LiOH and Li_2CO_3 (Ghorbanzade et al., 2024). To address this issue, doping with aluminum oxide (Al_2O_3) has been employed as a strategy to stabilize the cubic phase and reduce lithium volatilization. The proper Li/Al ratio plays a crucial role in controlling the formation of lithium-rich secondary phases, which in turn can enhance ionic conductivity (Hu et al., 2023). The homogeneity of precursors is also a critical factor in the synthesis of Al_2O_3-doped LLZO. Uniform precursor distribution helps regulate compositional and structural evolution during synthesis while minimizing the formation of unwanted secondary impurities (Parascos et al., 2022).

Under sintering conditions of 900°C for 4 hours, several additional phases such as $La(OH)_3$, Li_2ZrO_3, Al_2O_3, La_2ZrO_7, and LiO_2H_3 were found in Al_2O_3-doped LLZO. This can be attributed to several factors, including the high volatility of lithium (particularly in the form of Li_2CO_3), which disrupts the stoichiometry required for the formation of pure LLZO phases (Barin, 2008; Parascos et al., 2022). Consequently, phases such as La_2ZrO_7 (indicating lithium deficiency) and Li_2ZrO_3 (resulting from localized lithium excess) were formed (Barnwal et al., 2024; Bi et al., 2016; Montoya et al., 2024). Furthermore, during the sintering process, atmospheric moisture can react with lithium oxide and lanthanum oxide, forming hydroxide phases such as $La(OH)_3$ and LiO_2H_3. This phenomenon is commonly observed at intermediate temperatures such as 900°C (Okos et al., 2023; Rosen et al., 2021). The presence of Al_2O_3, introduced as a dopant to inhibit grain growth (Nagashima et al., 2008), may also remain as a separate phase if not evenly distributed throughout the mixture. These factors collectively influence the final phase composition, highlighting the critical need for strict control over synthesis conditions to obtain high-performance LLZO.

The cubic phase exhibits higher Li-ion conductivity but is thermodynamically unstable at ambient room temperature, tending to adopt a tetragonal structure (Enkhbayar & Kim, 2022; J. Wang et al., 2024). High-valence-element doping introduces vacancies, destabilizing the tetragonal phase and promoting the formation of the more stable cubic phase. Additionally, the introduction of lithium-ion vacancies enhances Li-ion conductivity, indicating that vacancy concentration and structural stability are key factors in phase transitions (You et al., 2024)

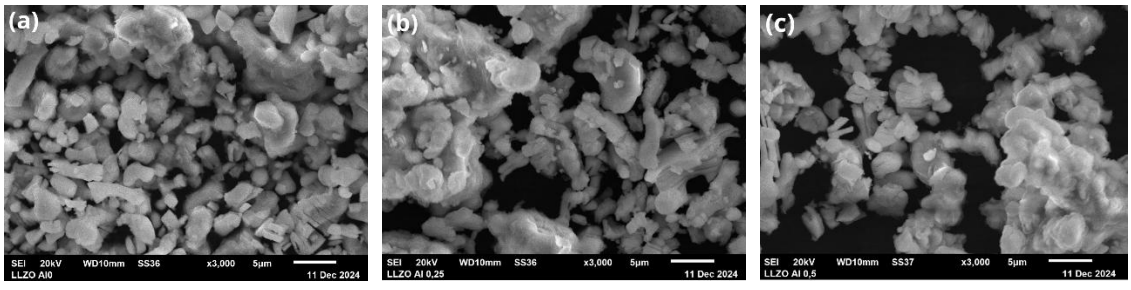

Figure 5 SEM micrographs of LLZO samples synthesized via solid-state reaction, captured at 3000× magnification: (a) pure-LLZO, (b) 0.25Al-LLZO, and (c) 0.5Al-LLZO.

The thermodynamic stability of the cubic and tetragonal phases of $Li_7La_3Zr_2O_{12}$ (LLZO) is influenced by temperature and CO_2 absorption factors. The tetragonal phase transforms into a non-quenchable cubic phase at approximately 650°C, with reversibility observed during heating and cooling cycles. Furthermore, CO_2 absorption, particularly around 200°C, can induce the transformation of the tetragonal phase into a low-temperature cubic phase. In contrast, the stability of the cubic phase is enhanced by Al substitution, which facilitates the formation of Li vacancies necessary for phase stabilization (Matsui et al., 2014). Dopants such as Al occupy critical Li at 24d sites, impeding diffusion

and reducing the effective vacancy concentration, collectively impacting phase stability and conductivity (You et al., 2024). A critical concentration of 0.4–0.5 Li vacancies per formula unit is required to stabilize the cubic phase. Additionally, the presence of adventitious Al during processing may influence phase stability by introducing additional Li vacancies. Insufficient doping results in a mixture of cubic and tetragonal phases, highlighting the crucial role of vacancy concentration in phase stability (Serhan et al., 2019).

3.3 Morphology of LLZO:Al Solid Electrolyte Material Observed Using Scanning Electron Microscopy (SEM)

The Scanning Electron Microscopy (SEM) analysis in this experiment, involving pure-LLZO, 0.25Al-LLZO, and 0.5Al-LLZO samples, was conducted at the Nuclear Characterization Laboratory, Sub-Laboratory of Advanced Nuclear Materials, BRIN KST BJ. Habibie, Serpong. The morphology of the Al_2O_3-doped $Li_7La_3Zr_2O_{12}$ (LLZO) solid electrolyte powder, sintered at 900°C for 4 hours, is depicted in Figures 5, 6, and 7. Figure 5a, 5b, and 5c show the morphology of the pure-LLZO sample at magnifications of 1000x, 3000x, and 5000x, respectively, while Figure 5d shows the grain size distribution of the pure-LLZO sample at 5000x magnification. Figure 6a, 6b, and 6c show the morphology of the 0.25Al-LLZO sample at magnifications of 1000x, 3000x, and 5000x, respectively, while Figure 6d shows the grain size distribution of the 0.25Al-LLZO sample at 3000x magnification. Figure 7a, 7b, and 7c show the morphology of the 0.5Al-LLZO sample at magnifications of 1000x, 3000x, and 5000x, respectively, while Figure 7d shows the grain size distribution of the 0.5Al-LLZO sample at 3000x magnification.

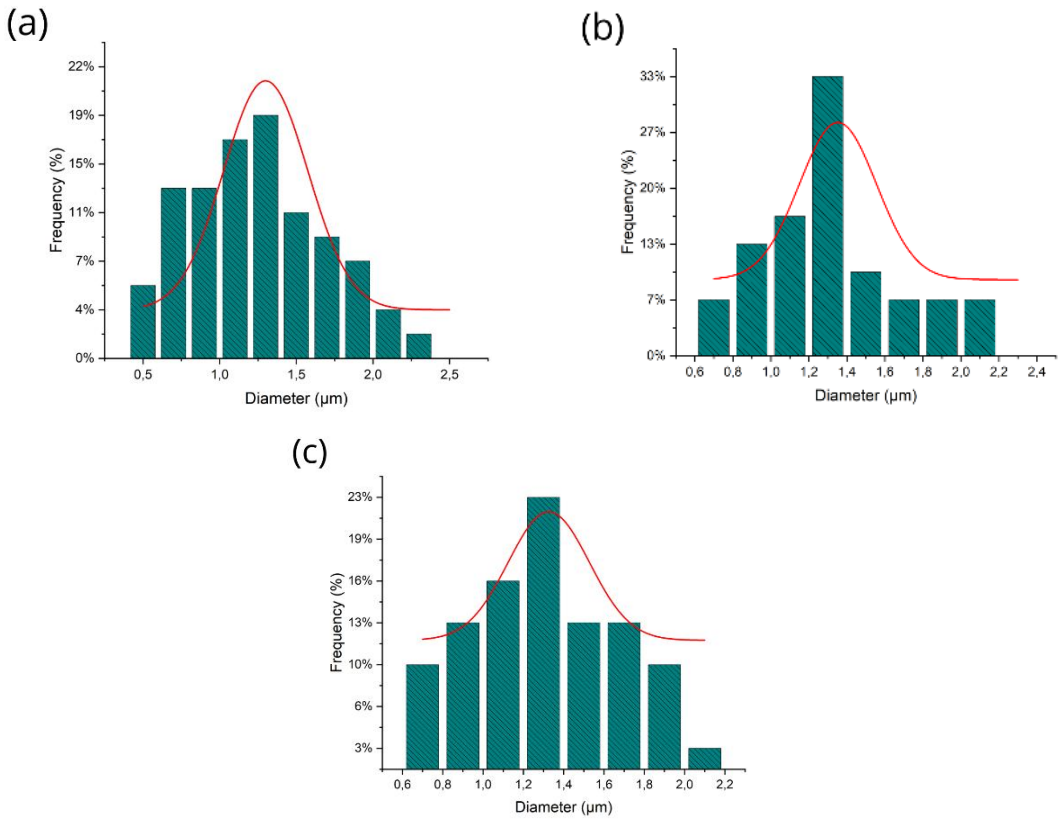

Figure 6 Grain size distribution histograms of LLZO samples obtained from SEM image analysis: (a) pure-LLZO, (b) 0.25Al-LLZO, and (c) 0.5Al-LLZO.

Figures 5 depict particle agglomeration with irregular shapes. In the pure-LLZO sample, large grains with varying sizes are prominent, reflecting suboptimal densification. The rough surface and noticeable porosity further indicate incomplete sintering. In the 0.25Al-LLZO sample, the surface appears smoother, signifying improved densification, though not yet fully optimized. The degree of

agglomeration is reduced compared to pure-LLZO, although clusters of larger particles are still evident. The 0.5Al-LLZO sample demonstrates the finest particle structure and the most uniform size distribution among the three samples. A denser surface and fewer pores indicate a more effective sintering process. Table 2 shows that the 0.5Al-LLZO sample has the highest density, measured at 5.07 g/cm³. The grain diameters for each sample are as follows: pure-LLZO with 1.25 ± 0.06 µm, 0.25Al-LLZO with 1.35 ± 0.1 µm, and 0.5Al-LLZO with 1.33 ± 0.12 µm. The comparison of grain diameters for LLZO:Al samples sintered at 900°C for 4 hours is presented in Figure 6 and Table 4.

Table 4 Grain Diameters of LLZO:Al Samples Sintered at 900°C for 4 hours

No.	Sample	$\bar{X}$	ΔX
1.	Pure-LLZO	1.2	0.06
2.	0.25Al-LLZO	1.3	0.10
3.	0.5Al-LLZO	1.3	0.12

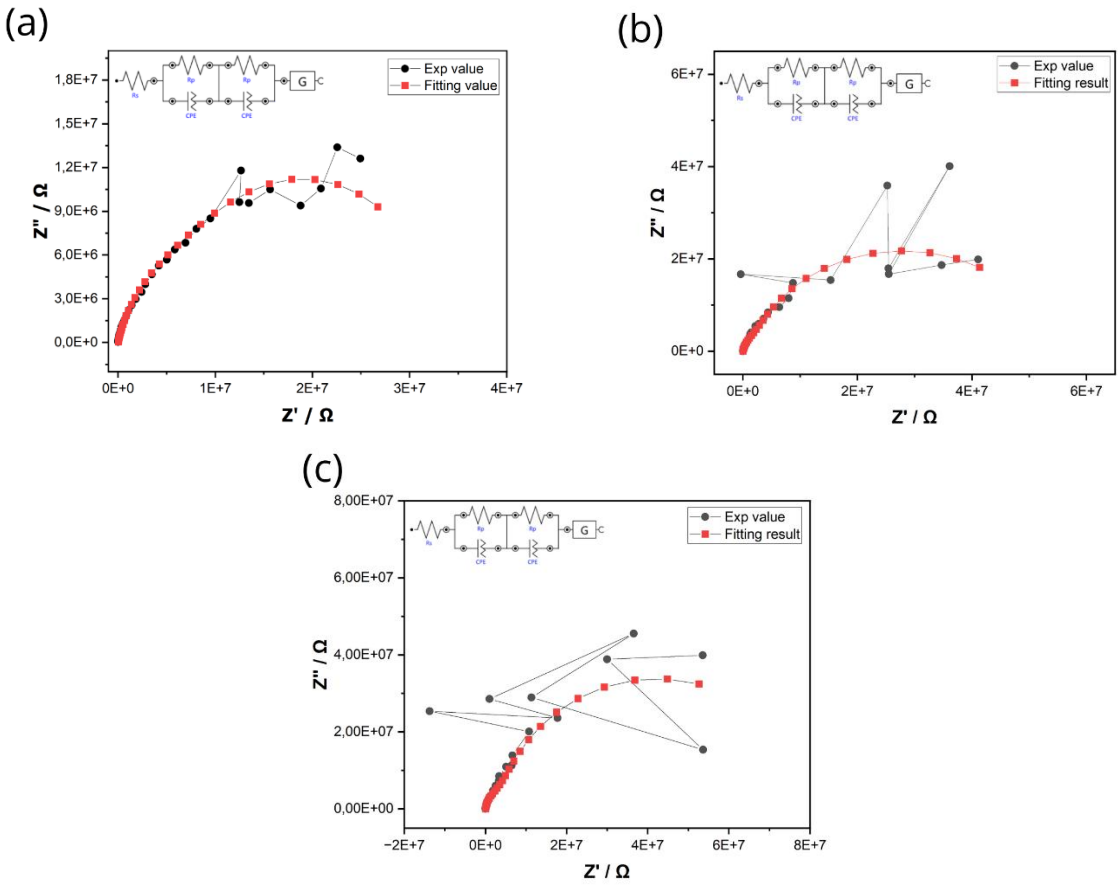

Figure 7 The impedance data with the corresponding fitting curve (red) and an equivalent circuit shown in the inset for (a) pure-LLZO, (b) 0.25Al-LLZO, and (c) 0.5Al-LLZO.

The grain diameter measurements for pure-LLZO show the smallest average value compared to the LLZO:Al samples. For the 0.25Al-LLZO and 0.5Al-LLZO samples, the grain sizes are larger than those of the pure-LLZO sample, which shows that the addition of Al_2O_3 results in larger grain diameters compared to samples without Al_2O_3. This increase is likely due to particle aggregation or clumping. During sintering, Al_2O_3 dopants may not be uniformly dispersed, leading to the formation of large agglomerates or clusters. As a result, the measured grain diameters reflect these aggregates rather than individual grains. In conventional sintering, dopants like Al_2O_3 can serve as grain growth inhibitors when concentrated at grain boundaries (Nagashima et al., 2008). However, at higher concentrations

(e.g., 0.25 and 0.5), uneven dopant distribution can localize sintering energy in specific areas, encouraging the formation of large particle agglomerates (Matsui et al., 2006; Najafkhani et al., 2021). Moreover, the longer heating times typically used in conventional sintering can facilitate secondary grain growth, especially when grain boundaries are unstable (Paredes-Goyes et al., 2021; Qin et al., 2022; Stanciu et al., 2001). This prolonged exposure may exacerbate dopant inhomogeneity, further contributing to the development of larger grain structures and reducing the overall uniformity of the material.

3.4 Impedance Characteristics of LLZO:Al Solid Electrolyte Cells Analyzed Using Electrochemical Impedance Spectroscopy (EIS)

The Nyquist plot obtained from Electrochemical Impedance Spectroscopy (EIS) measurements presents the horizontal axis representing Z' (real impedance) and the vertical axis representing Z'' (imaginary impedance). Figure 7a-c shows a Nyquist plot of the impedance data for pure-LLZO, 0.25Al-LLZO, and 0.5Al-LLZO, respectively, with the corresponding fitting curve (red) and an equivalent circuit shown in the inset. The fitted electrochemical impedance spectroscopy (EIS) parameters of pure and Al-doped LLZO samples are presented in Table 5. Rs represents the bulk resistance, while Rp_1 and Rp_2 correspond to the grain and grain boundary resistances, respectively. CPE_1 and CPE_2 denote the constant phase elements associated with the bulk and grain boundary responses, respectively, as obtained from equivalent circuit fitting.

Table 5 Fitted EIS parameters of pure and Al-doped LLZO samples, including bulk resistance (Rs), grain and grain boundary resistances (Rp_1, Rp_2), and constant phase elements (CPE_1, CPE_2).

No.	Sample	Rs (ohm)	Rp_1 (ohm)	Rp_2 (ohm)	CPE_1	CPE_2
1.	Pure-LLZO	802	6450000	27900000	0.803	0.815
2.	0.25Al-LLZO	1540	52500000	1830000	0.879	0.95
3.	0.5Al-LLZO	2300	77300000	3800000	0.912	0.93

In the equivalent circuit shown in Figure 7, several key electrical elements are used to model the impedance response of the LLZO material tested using Electrochemical Impedance Spectroscopy (EIS). These electrical elements include R_s (Series Resistance), R_p (Polarization Resistance or Grain Boundary Resistance), and CPE (Constant Phase Element). R_s represents the series resistance, accounting for the electrodes' intrinsic resistance and electrode-electrolyte interface. R_p corresponds to the resistance associated with charge transfer impediments within the material, originating from grain boundaries or the bulk region of the LLZO. CPE is a constant phase element used as a substitute for an ideal system capacitor. From the circuit shown in Figures 8a, 8b, and 8c, the presence of two R_p and two CPE elements suggests two different conduction mechanisms in the LLZO sample, namely ion transport in the bulk and across the grain boundaries. This aligns with the fitting results, which exhibit two semicircles on the Nyquist plot, though they are not highly visible due to their imperfect shape. The LLZO ionic conductivity value obtained for pure-LLZO is $9.54 \times 10^{-10}\ S/cm$, for 0.25Al-LLZO is $2.83 \times 10^{-9}\ S/cm$, and for 0.5Al-LLZO is $1.38 \times 10^{-9}\ S/cm$, with the highest conductivity value in the 0.25Al-LLZO sample.

4. CONCLUSION

The synthesis of Al-doped $Li_7La_3Zr_2O_{12}$ (LLZO:Al) via solid-state reaction using a one-step heat treatment at 900 °C for 4 hours successfully yielded the tetragonal LLZO phase, along with minor secondary phases including $La(OH)_3$, $LiIO_3$, Li_2ZrO_3, and Al_2O_3. The resulting materials exhibited grain sizes in the 1.2–1.3 µm range and densities between 5.02 and 5.07 g/cm³, with the highest density observed in the 0.5Al-LLZO sample. The incorporation of Al_2O_3 effectively enhanced densification under conventional sintering conditions. Ionic conductivity varied from 9.54×10^{-10} to 1.38×10^{-9} S/cm, with the 0.25Al-LLZO sample achieving the highest value of 2.83×10^{-9} S/cm. These results demonstrate that a single-step heat treatment at 900 °C for 4 hours provides sufficient densification while limiting lithium volatilization, contributing to the stability of the LLZO phase.

Despite these advantages, relatively high resistance and secondary phases remain challenges in further improving ionic conductivity. Future work should optimize the Al_2O_3 doping concentration, particularly in the 0.25–0.5 mol range, or employ co-doping strategies to balance densification and conductivity. Additionally, alternative sintering approaches such as Spark Plasma Sintering (SPS) are recommended to enhance densification, reduce grain boundary resistance, and suppress secondary phase formation.

ACKNOWLEDGEMENT

The authors would like to thank the Direktorat Riset, Teknologi, dan Pengabdian Kepada Msyarakat (DRTPM) Direktorat Jenderal Pendidikan Tinggi, Riset, dan Teknologi (Ditjen Diktiristek) Kementerian Pendidikan, Kebudayaan, Riset, dan Teknologi (Kemendikbudristek) for providing the funding that made this research possible. Gratitude is also extended to Universitas Dirgantara Marsekal Suryadarma (Unsurya) and the National Research and Innovation Agency (BRIN) KST BJ Advanced Materials Research Center, Habibie Serpong, for their laboratory support, which enabled this important research to be conducted effectively.

REFERENCE

Barin, I. (2008). *Thermochemical Data of Pure Substances, 3rd Edition* (3rd Edition). Wiley. https://doi.org/10.1002/9783527619825

Barnwal, A., Bais, P., Balakrishna, M., Nair, R. K. S., Ravendran, R., & Kaushal, A. (2024). Recovery of Lithium, Cobalt, and Graphite Contents from Black Mass of LCO-Based Discarded Li-Ion Batteries. *Mining, Metallurgy & Exploration*, *41*(6), 3517–3527. https://doi.org/10.1007/s42461-024-01043-w

Bi, Y., Wang, T., Liu, M., Du, R., Yang, W., Liu, Z., Peng, Z., Liu, Y., Wang, D., & Sun, X. (2016). Stability of Li2CO3 in cathode of lithium ion battery and its influence on electrochemical performance. *RSC Advances*, *6*(23), 19233–19237. https://doi.org/10.1039/c6ra00648e

Enkhbayar, E., & Kim, J. (2022). Study of Codoping Effects of Ta5+ and Ga3+ on Garnet Li7La3Zr2O12. *ACS Omega*, *7*(50), 47265–47273. https://doi.org/10.1021/acsomega.2c06544

Ghorbanzade, P., López-Aranguren, P., & López del Amo, J. M. (2024). A Vision for LLZO Carbonate Formation: Perspectives on Surface Treatment Approaches and Characterization Techniques. *ChemElectroChem*, *11*(11), 1–7. https://doi.org/10.1002/celc.202400136

Han, L., Lehmann, M. L., Zhu, J., Liu, T., Zhou, Z., Tang, X., Heish, C. Te, Sokolov, A. P., Cao, P., Chen, X. C., & Saito, T. (2020). Recent Developments and Challenges in Hybrid Solid Electrolytes for Lithium-Ion Batteries. In *Frontiers in Energy Research* (Vol. 8, pp. 1–19). Frontiers Media S.A. https://doi.org/10.3389/fenrg.2020.00202

Heywood, S., Lessmeier, M., Driscoll, D., & Sofie, S. (2023). Tailoring solid-state synthesis routes for high confidence production of phase pure, low impedance Al-LLZO. *Journal of the American Ceramic Society*, *106*(5), 2786–2796. https://doi.org/https://doi.org/10.1111/jace.18994

Heywood, S., Sofie, S., & Driscoll, D. (2022). Solid State Synthesis of Aluminum Doped Li7La3Zr2O12 Garnet with Enhanced Thermal Processing Stability. *ECS Meeting Abstracts*, *MA2022-01*(6), 2427. https://doi.org/10.1149/MA2022-0162427mtgabs

Hu, X., Chen, S., Wang, Z., Chen, Y., Yuan, B., Zhang, Y., Liu, W., & Yu, Y. (2023). Microstructure of the Li–Al–O Second Phases in Garnet Solid Electrolytes. *Nano Letters*, *23*(3), 887–894. https://doi.org/10.1021/acs.nanolett.2c04135

Ihrig, M., Mishra, T. P., Scheld, W. S., Häuschen, G., Rheinheimer, W., Bram, M., Finsterbusch, M., & Guillon, O. (2021). Li7La3Zr2O12 solid electrolyte sintered by the ultrafast high-temperature method. *Journal of the European Ceramic Society*, *41*(12), 6075–6079. https://doi.org/https://doi.org/10.1016/j.jeurceramsoc.2021.05.041

Il'ina, E. A., Raskovalov, A. A., & Reznitskikh, O. G. (2019). Thermodynamic properties of solid electrolyte Li7La3Zr2O12. *The Journal of Chemical Thermodynamics*, *128*, 68–73. https://doi.org/https://doi.org/10.1016/j.jct.2018.08.009

Karuppiah, D., Komissarenko, D., Yüzbasi, N. S., Liu, Y., Warriam Sasikumar, P. V., Hadian, A., Graule, T., Clemens, F., & Blugan, G. (2023). A Facile Two-Step Thermal Process for Producing a Dense, Phase-Pure, Cubic Ta-Doped Lithium Lanthanum Zirconium Oxide Electrolyte for Upscaling. *Batteries*, *9*(11), 554–565. https://doi.org/10.3390/batteries9110554

Kiyek, V., Schwab, C., Scheld, W. S., Roitzheim, C., Lindner, A., Menesklou, W., Finsterbusch, M., Fattakhova-Rohlfing, D., & Guillon, O. (2024). Direct Precursor Route for the Fabrication of LLZO Composite Cathodes for Solid-State Batteries. *Advanced Science*, *11*(42), 1–11. https://doi.org/10.1002/advs.202404682

Lan, W., Fan, H., Lau, V. W., Zhang, J., Zhang, J., Zhao, R., & Chen, H. (2020). Realizing Li7La3Zr2O12 garnets with high Li+ conductivity and dense microstructures by Ga/Nb dual substitution for lithium solid-state battery applications. *Sustainable Energy Fuels*, *4*(4), 1812–1821. https://doi.org/10.1039/C9SE01162E

Li, C., Wu, Y., Lv, Z., Peng, J., Liu, J., Zheng, X., Wu, Y., Tang, W., Gong, Z., & Yang, Y. (2024). Binary anion and cation co-doping enhance sulfide solid electrolyte performance for all-solid-state lithium batteries. *Energy Materials*, *4*(1), 1–14. https://doi.org/10.20517/energymater.2023.78

Lotsch, B. V., & Maier, J. (2017). Relevance of solid electrolytes for lithium-based batteries: A realistic view. *Journal of Electroceramics*, *38*(2–4), 128–141. https://doi.org/10.1007/s10832-017-0091-0

Luo, Y., Rao, Z., Yang, X., Wang, C., Sun, X., & Li, X. (2024). Safety Concerns in Solid-State Lithium Batteries: From Materials to Devices. *Energy & Environmental Science*, *17*, 7543–7565. https://doi.org/10.1039/d4ee02358g

Ma, C., Grandhi, M., Mallory, P., Liu, Z., Li, B., & Kang, B. (2024). Directed energy deposited SS316L with nano-Y2O3 additions: powder processing, microstructure, and mechanical properties. *Progress in Additive Manufacturing*, *10*, 2831–2846. https://doi.org/10.1007/s40964-024-00787-7

Machín, A., Morant, C., & Márquez, F. (2024). Advancements and Challenges in Solid-State Battery Technology: An In-Depth Review of Solid Electrolytes and Anode Innovations. In *Batteries* (Vol. 10, Issue 1). Multidisciplinary Digital Publishing Institute (MDPI). https://doi.org/10.3390/batteries10010029

Matsui, K., Ohmichi, N., Ohgai, M., Yoshida, H., & Ikuhara, Y. (2006). Effect of alumina-doping on grain boundary segregation-induced phase transformation in yttria-stabilized tetragonal zirconia polycrystal. *Journal of Materials Research*, *21*(9), 2278–2289. https://doi.org/10.1557/jmr.2006.0274

Matsui, M., Takahashi, K., Sakamoto, K., Hirano, A., Takeda, Y., Yamamoto, O., & Imanishi, N. (2014). Phase stability of a garnet-type lithium ion conductor Li 7La3Zr2O12. *Dalton Transactions*, *43*(3), 1019–1024. https://doi.org/10.1039/c3dt52024b

Montoya, S. T., Shanto, S. A. H., & Walker, R. A. (2024). Lithium Volatilization and Phase Changes during Aluminum-Doped Cubic Li6.25La3Zr2Al0.25O12 (c-LLZO) Processing. *Crystals*, *14*(9), 795. https://doi.org/10.3390/cryst14090795

Nagashima, M., Motoike, K., & Hayakawa, M. (2008). Fabrication and optical characterization of high-density Al_2O_3 doped with slight MnO dopant. *Journal of the Ceramic Society of Japan*, *116*(1353), 645–648. https://doi.org/10.2109/jcersj2.116.645

Najafkhani, F., Kheiri, S., Pourbahari, B., & Mirzadeh, H. (2021). Recent advances in the kinetics of normal/abnormal grain growth: a review. *Archives of Civil and Mechanical Engineering*, *21*(1), 29. https://doi.org/10.1007/s43452-021-00185-8

Neises, J., Scheld, W. S., Seok, A. R., Lobe, S., Finsterbusch, M., Uhlenbruck, S., Schmechel, R., & Benson, N. (2022). Study of thermal material properties for Ta- and Al-substituted Li7La3Zr2O12 (LLZO) solid-state electrolyte in dependency of temperature and grain size. *Journal of Materials Chemistry A*, *10*(22), 12177–12186. https://doi.org/10.1039/d2ta00323f

Okos, A., Ciobota, C. F., Motoc, A. M., & Piticescu, R. R. (2023). Review on Synthesis and Properties of Lithium Lanthanum Titanate. In *Materials* (Vol. 16, Issue 22). Multidisciplinary Digital Publishing Institute (MDPI). https://doi.org/10.3390/ma16227088

Parascos, K., Watts, J. L., Alarco, J. A., Chen, Y., & Talbot, P. C. (2022). Compositional and structural control in LLZO solid electrolytes. *RSC Advances*, *12*(36), 23466–23480. https://doi.org/10.1039/d2ra03303h

Paredes-Goyes, B., Jauffres, D., Missiaen, J.-M., & Martin, C. L. (2021). Grain growth in sintering: A discrete element model on large packings. *Acta Materialia*, *218*, 117182. https://doi.org/https://doi.org/10.1016/j.actamat.2021.117182

Qin, M., Shivakumar, S., & Luo, J. (2022). *High-temperature stable refractory high-entropy nanoalloys with enhanced sinterability*. *11*, 1–26. https://doi.org/10.48550/arXiv.2212.10932

Raju, M. M., Altayran, F., Johnson, M., Wang, D., & Zhang, Q. (2021). Crystal Structure and Preparation of Li7La3Zr2O12 (LLZO) Solid-State Electrolyte and Doping Impacts on the Conductivity: An Overview. In *Electrochem* (Vol. 2, Issue 3, pp. 390–414). Multidisciplinary Digital Publishing Institute (MDPI). https://doi.org/10.3390/electrochem2030026

Rangasamy, E., Wolfenstine, J., & Sakamoto, J. (2012). The role of Al and Li concentration on the formation of cubic garnet solid electrolyte of nominal composition Li 7La 3Zr 2O 12. *Solid State Ionics*, *206*, 28–32. https://doi.org/10.1016/j.ssi.2011.10.022

Rosen, M., Ye, R., Mann, M., Lobe, S., Finsterbusch, M., Guillon, O., & Fattakhova-Rohlfing, D. (2021). Controlling the lithium proton exchange of LLZO to enable reproducible processing and performance optimization. *Journal of Materials Chemistry A*, *9*(8), 4831–4840. https://doi.org/10.1039/d0ta11096e

Salimkhani, H., Yurum, A., & Gursel, S. A. (2021). A glance at the influence of different dopant elements on Li7La3Zr2O12 garnets. *Ionics*, *27*(9), 3673–3698. https://doi.org/10.1007/s11581-021-04152-4

Serhan, M., Sprowls, M., Jackemeyer, D., Long, M., Perez, I. D., Maret, W., Tao, N., & Forzani, E. (2019). Total iron measurement in human serum with a smartphone. *AIChE Annual Meeting, Conference Proceedings*, *2019-November*. https://doi.org/10.1039/x0xx00000x

Sharifi, O., Golmohammad, M., Soozandeh, M., & Mehranjani, A. S. (2023). Improved Ga-doped Li7La3Zr2O12 garnet-type solid electrolytes for solid-state Li-ion batteries. *Journal of Solid State Electrochemistry*, *27*(9), 2433–2444. https://doi.org/10.1007/s10008-023-05522-w

Stanciu, L. A., Kodash, V. Y., & Groza, J. R. (2001). Effects of heating rate on densification and grain growth during field-assisted sintering of α-Al2O3 and MoSi2 powders. *Metallurgical and Materials Transactions A: Physical Metallurgy and Materials Science*, *32*(10), 2633–2638. https://doi.org/10.1007/s11661-001-0053-6

Tsai, C. L., Ma, Q., Dellen, C., Lobe, S., Vondahlen, F., Windmüller, A., Grüner, D., Zheng, H., Uhlenbruck, S., Finsterbusch, M., Tietz, F., Fattakhova-Rohlfing, D., Buchkremer, H. P., & Guillon, O. (2019). A garnet structure-based all-solid-state Li battery without interface modification: Resolving incompatibility issues on positive electrodes. *Sustainable Energy and Fuels*, *3*(1), 280–291. https://doi.org/10.1039/c8se00436f

Wang College Park MD (United States)], C. [Univ. of M., Fu College Park MD (United States); Univ. of Delaware Newark DE (United States)] (ORCID:000000034963615X), K. [Univ. of M., Kammampata AB (Canada)], S. P. [Univ. of C., McOwen College Park MD (United States)], D. W. [Univ. of M., Samson AB (Canada)], A. J. [Univ. of C., Zhang College Park MD (United States)], L. [Univ. of M., Hitz College Park MD (United States)], G. T. [Univ. of M., Nolan College Park MD (United States)], A. M. [Univ. of M., Wachsman College Park MD (United States)] (ORCID:0000000206671927), E. D. [Univ. of M., Mo College Park MD (United States)] (ORCID:0000000281624629), Y. [Univ. of M., Thangadurai AB (Canada)] (ORCID:0000000162566307), V. [Univ. of C., & Hu College Park MD (United States)] (ORCID:0000000294569315), L. [Univ. of M. (2020). *Garnet-Type Solid-State Electrolytes: Materials, Interfaces, and Batteries*. *120*. https://doi.org/https://doi.org/10.1021/acs.chemrev.9b00427

Wang, J., Li, X., Wang, X., Liu, G., Yu, W., Dong, X., & Wang, J. (2024). The synergistic effects of dual substitution of Bi and Ce on ionic conductivity of Li7La3Zr2O12 solid electrolyte. *Ceramics International*, *50*(4), 6472–6480. https://doi.org/https://doi.org/10.1016/j.ceramint.2023.11.391

Wang, S., La Monaca, A., & Demopoulos, G. P. (2025). Composite solid-state electrolytes for all solid-state lithium batteries: progress, challenges and outlook. In *Energy Advances* (Vol. 4, Issue 1, pp. 11–36). Royal Society of Chemistry. https://doi.org/10.1039/d4ya00542b

Wood, M., Gao, X., Shi, R., Heo, T. W., Espitia, J. A., Duoss, E. B., Wood, B. C., & Ye, J. (2020). *Exploring the relationship between solvent-assisted ball milling, particle size, and sintering temperature in garnet-type solid electrolytes*. *484*, 1–11. https://doi.org/10.1016/j.jpowsour.2020.229252

Woolley, H. M., & Vargas-Barbosa, N. M. (2022). Hybrid solid electrolyte-liquid electrolyte systems for (almost) solid-state batteries: Why, how, and where to? In *Journal of Materials Chemistry A* (Vol. 11, Issue 3, pp. 1083–1097). Royal Society of Chemistry. https://doi.org/10.1039/d2ta02179j

Wu, J., Lu, Y., Wu, H., Luo, Q., Bai, Z., & Li, J. (2023). Preparation and electrochemical properties of LLZO co-doping with Al and Ti for all solid-state battery. *Journal of Solid State Electrochemistry*, *27*(9), 2499–2507. https://doi.org/10.1007/s10008-023-05532-8

Xue, W., Yang, Y., Yang, Q., Liu, Y., Wang, L., Chen, C., & Cheng, R. (2018). The effect of sintering process on lithium ionic conductivity of Li6.4Al0.2La3Zr2O12 garnet produced by solid-state synthesis. *RSC Advances*, *8*(24), 13083–13088. https://doi.org/10.1039/c8ra01329b

Yoon, S. A., Oh, N. R., Yoo, A. R., Lee, H. G., & Lee, H. C. (2017). Preparation and Characterization of Ta-substituted Li7La3Zr2-xO12 Garnet Solid Electrolyte by Sol-Gel Processing. *J. Korean Ceram. Soc*, *54*(4), 278–284. https://doi.org/10.4191/kcers.2017.54.4.02

You, Y., Zhang, D., Cao, X., Lü, T.-Y., Zhu, Z.-Z., & Wu, S. (2024). Exploring high-valence element doping in LLZO electrolytes: Effects on phase transition and lithium-ion conductivity. *Journal of Power Sources*, *612*, 234831. https://doi.org/https://doi.org/10.1016/j.jpowsour.2024.234831

Zhao, W., Yi, J., He, P., & Zhou, H. (2019). Solid-State Electrolytes for Lithium-Ion Batteries: Fundamentals, Challenges and Perspectives. In *Electrochemical Energy Reviews* (Vol. 2, Issue 4, pp. 574–605). Springer Science and Business Media B.V. https://doi.org/10.1007/s41918-019-00048-0